Asociación Argentina
de Mecánica Computacional

Mecánica Computacional Vol XXIX, págs. 3371-3387 (artículo completo)
Eduardo Dvorkin, Marcela Goldschmit, Mario Storti (Eds.)
Buenos Aires, Argentina, 15-18 Noviembre 2010

FINITE VOLUME SIMULATION OF SOLAR DARK LANES STRUCTURES

Sergio Elaskar[a,b], **Andrea Costa**[a,b], **Walkiria Schulz**[a] **and Guillermo Cid**[a]

[a]*Universidad Nacional de Córdoba, Departamento de Aeronáutica y CONICET.*
Avenida Vélez Sarfield 1611, Córdoba, Argentina, 5000, selaskar@efn.uncor.edu

[b]*CONICET*

Key words: shock waves – Sun: corona – Sun: flares – Sun: magnet fields – Sun: oscillations.

Abstract. We integrate the ideal magnetogasdynamics equations to simulate dark void sunward moving structures in post-flare supra-arcades. We study the generation and evolution of the internal plasma instability to compare with observations and to gain insight into physical processes and characteristic parameters of these phenomena. The numerical approach uses a finite-volume method together the Harten–Yee total variation diminishing (TVD) scheme to integrate non-steady, one-dimensional magnetogasdynamics. Two set of numerical tests were carried out, one of them in the sunward radial direction and the another one transverse to the sun's magnetic field. We can numerically reproduce dark void solar observations. We show that the dark lanes are plasma vacuums generated by the bouncing and interfering of shocks and expansion waves produced by a localized deposition of energy. This energy deposition is modeled as a pressure perturbation. The pressure perturbation produces non-linear waves that compose the plasma void structures, with the same functional sunward decreasing phase speed and constancy with height of the period, as those determined by the observations.

Copyright © 2010 Asociación Argentina de Mecánica Computacional http://www.amcaonline.org.ar

1 1 INTRODUCTION

Dark sunward sinuous lanes moving along a fan of rays above post–flare loops towards a supra–arcade have been extensively studied (McKenzie 2000; Innes *et al.* 2003a,b; Asai et al. 2004; McKenzie and Savage 2009). The down moving structures observed at 40Mm - 60Mm heights above the top of arcades, with a decelerating speed in the range of 50 - 1000km/s were interpreted as sunward voided flows generated by reconnection processes developed by a current sheet above the flare arcade. Verwichte *et al.* (2005) analyzed transverse to the magnetic field oscillations associated with sunward dark lanes in a post–flare supra–arcade. They found that the phase speeds and the displacement amplitudes, of observational dark lanes of a kink–like type, decrease as they propagate downwards while the period remains constant with height.

In Costa *et al*. (2009) and in Schulz *et al*. (2010) by the integration of one dimensional and time dependent magnetogasdynamics ideal equations, we presented a new scenario to numerically give account of the observational dark voids described in Verwichte *et al.* (2005). We simulated the effects of an initial impulsive and localized deposition of energy in a plasma structured by sunward magnetic field lines. The impulsive phase was modeled by a pressure perturbation that initiates two main different type of processes, a fundamentally hydrodynamic shock pattern directed sunwards and a perpendicular magnetic shock one, i.e., transversal to the magnetic field. The two patterns were supposed to be partially independent processes linked by their common origin and background magnetic and density conditions. The independence of the two dynamics was justified due to the far more effective conductive energy transport along field lines than across them.

In the transverse direction *y*, the resulting interactions of nonlinear waves that rebound in the denser external medium composes and sustains, in accordance with observational characteristic times of the phenomenon, a density structure with a central void resembling a kink–like mode or a sausage–like mode.

The same reference values were used as initial conditions to simulate the sunward evolution. We could reproduce the observational data showing that initially two opposite shock evolving fronts are produced. One evolves towards the sun surface until is absorbed, and the other is forced to rebound upwardly resembling the action of the reconnection site.

In Schulz, *et al.* (2010) we analyze the sensibility of the phenomena to different initial conditions and, subject to the limitations of our modeling, we show the functional dependence of the amplitude, the phase speed and the periods with plasma parameters. We estimate the range of possible physical conditions that could give rise to the voided phenomena, i.e., magnetic field intensity and triggering pulse pressure.

In this paper we present details about the implemented numerical scheme to evaluate the dynamics of the solar dark lanes. To simulate time dependent magnetogasdynamics flows it is used a software method developed by us (Elaskar and Brito, 2001). The implemented equations are continuity, momentum, energy and magnetic induction equations together with the state equation forming a system of partial hyperbolic differential equations. The numerical approach is based on an approximate Riemann solver with a high resolution TVD technique. The eight-wave technique introduced by Powell (1995) is used and the eigenvectors are normalized according to Zarachay, *et al.* (1994) and Roe (1996). The accuracy of the technique was verified by simulations of the Riemann problem introduced by Brio and Wu and the Hartmann flows (Maglione *et al*. 2007).

Copyright © 2010 Asociación Argentina de Mecánica Computacional http://www.amcaonline.org.ar

2 MAGNETOGASDYNAMICS EQUATIONS

The equations of non-dimensional transient real MGD in conservative form are given by (Goldston and Rutherford, 2003; D'Ambrosio and Giordano, 2004).

$$\frac{\partial}{\partial t}\begin{bmatrix}\rho\\ \rho\boldsymbol{u}\\ \boldsymbol{B}\\ e\end{bmatrix}+\nabla\cdot\begin{bmatrix}\rho\boldsymbol{u}\\ \rho\boldsymbol{u}\boldsymbol{u}-\boldsymbol{B}\boldsymbol{B}+\boldsymbol{I}\left(p+\frac{1}{2}B^2\right)\\ \boldsymbol{u}\boldsymbol{B}-\boldsymbol{B}\boldsymbol{u}\\ \left(e+p+\frac{B^2}{2}\right)\boldsymbol{u}-\left(\boldsymbol{B}\cdot\boldsymbol{u}\right)\boldsymbol{B}\end{bmatrix}=\nabla\cdot\begin{bmatrix}0\\ \frac{\boldsymbol{\tau}}{R_e A_l}\\ \frac{\boldsymbol{E}_r}{L_u A_l}\\ \frac{\boldsymbol{u}\cdot\tau}{R_e A_l}-\frac{\left[\boldsymbol{\eta}\cdot\left(\nabla\times\boldsymbol{B}\right)\right]\times\boldsymbol{B}}{L_u A_l}+\frac{\boldsymbol{k}\cdot\nabla T}{P_e A_l}\end{bmatrix} \tag{1}$$

where ρ, $\boldsymbol{u}$,e ,p, T are the density, velocity, total energy, pressure and temperature of plasma respectively. B is the magnetic field, K thermal conductivity, η electrical resistive and τ viscous stress. R_e, A_l, L_u, P_e are the Reynolds, Alfvén, Lundquist and Peclet numbers.

The ideal MGD equations accurately describe the macroscopic dynamics of perfectly conducting plasma. This system expresses conservation of mass, momentum, energy, and magnetic flux and conform a nonlinear conservative system of eight partial differential equations. The equations of non-dimensional ideal one-fluid MGD in conservative form are given by (D'Ambrosio and Giordano, 2004);

$$\frac{\partial}{\partial t}\begin{bmatrix}\rho\\ \rho\boldsymbol{u}\\ \boldsymbol{B}\\ e\end{bmatrix}+\nabla\cdot\begin{bmatrix}\rho\boldsymbol{u}\\ \rho\boldsymbol{u}\boldsymbol{u}-\boldsymbol{B}\boldsymbol{B}+\boldsymbol{I}\left(p+\frac{1}{2}B^2\right)\\ \boldsymbol{u}\boldsymbol{B}-\boldsymbol{B}\boldsymbol{u}\\ \left(e+p+\frac{1}{2}B^2\right)\boldsymbol{u}-\left(\boldsymbol{B}\cdot\boldsymbol{u}\right)\boldsymbol{B}\end{bmatrix}=\boldsymbol{0} \tag{2}$$

To close de system, the perfect gas state equation is introduced, so the specific internal energy depends on the temperature only. Then the total energy results,

$$e=\frac{p}{\gamma-1}+\rho\ \frac{\boldsymbol{u}\cdot\boldsymbol{u}}{2}+\frac{\boldsymbol{B}\cdot\boldsymbol{B}}{2} \tag{3}$$

Using a Cartesian coordinate system Eq.(2), for two dimensions in quasi-linear form,) can be written as

$$\frac{\partial\boldsymbol{U}}{\partial t}+\left[A_c\right]\frac{\partial\boldsymbol{U}}{\partial x}+\left[B_c\right]\frac{\partial\boldsymbol{U}}{\partial y}=\boldsymbol{0} \tag{4}$$

with the state vector

$$\boldsymbol{U}=\left(\rho,\rho u_x,\rho u_y,\rho u_z,B_x,B_y,B_z,e\right)^T \tag{5}$$

where $[A_c]$ y $[B_c]$ are the Jacobian matrices. The evaluation of the eigenvalues and the eigenvectors is simpler using the conservative variables:

Copyright © 2010 Asociación Argentina de Mecánica Computacional http://www.amcaonline.org.ar

$$\boldsymbol{W} = \left(\rho, u_x, u_y, u_z, B_x, B_y, B_z, p\right)^T \tag{6}$$

To overcome the difficulties introduced by the null eigenvalue of the Jacobian matrices, the eight-wave technique introduced by Powell (1995) is used in this work. The modified Jacobian matrix $[A_p]$ (using primitive variables) is:

$$\left[A_p\right] = \begin{bmatrix} u_x & \rho & 0 & 0 & 0 & 0 & 0 & 0 \\ 0 & u_x & 0 & 0 & 0 & \frac{B_y}{\rho} & \frac{B_z}{\rho} & \frac{1}{\rho} \\ 0 & 0 & u_x & 0 & 0 & -\frac{B_x}{\rho} & 0 & 0 \\ 0 & 0 & 0 & u_x & 0 & 0 & -\frac{B_x}{\rho} & 0 \\ 0 & 0 & 0 & 0 & u_x & 0 & 0 & 0 \\ 0 & B_y & -B_x & 0 & 0 & u_x & 0 & 0 \\ 0 & B_z & 0 & -B_x & 0 & 0 & u_x & 0 \\ 0 & \gamma p & 0 & 0 & 0 & 0 & 0 & u_x \end{bmatrix} \tag{7}$$

The eigenvectors are normalized according to Zarachay *et al.* (1994) and Roe (1996). The resulting eigenvalues representing MGD waves are: “entropy wave”, “Alfvén waves”, “fast magneto-acoustic waves”, “slow magneto-acoustic waves” and “magnetic flux wave”. The expressions for these are:

-Entropy wave: $\lambda_e = u_x$.

$$\underset{\sim}{r}_e = \begin{Bmatrix} 1 \\ 0 \\ 0 \\ 0 \\ 0 \\ 0 \\ 0 \\ 0 \end{Bmatrix} \qquad \underset{\sim}{l}_e = \begin{Bmatrix} 1 \\ 0 \\ 0 \\ 0 \\ 0 \\ 0 \\ 0 \\ -\frac{1}{c^2} \end{Bmatrix} \tag{8}$$

-Alfvén waves: $\lambda_a = u_x \pm c_a$

Copyright © 2010 Asociación Argentina de Mecánica Computaciona

$$\underset{\sim}{r}_a^{\pm} = \frac{1}{\sqrt{2}} \begin{Bmatrix} 0 \\ 0 \\ -\beta_z \\ \beta_y \\ 0 \\ \pm\sqrt{\rho}\beta_z \\ \mp\sqrt{\rho}\beta_y \\ 0 \end{Bmatrix} \qquad \underset{\sim}{l}_a^{\pm} = \frac{1}{\sqrt{2}} \begin{Bmatrix} 0 \\ 0 \\ -\beta_z \\ \beta_y \\ 0 \\ \pm\dfrac{\beta_z}{\sqrt{\rho}} \\ \mp\dfrac{\beta_y}{\sqrt{\rho}} \\ 0 \end{Bmatrix} \tag{9}$$

-Fast magneto-acoustic waves: $\lambda_f = u_x \pm c_f$

$$\underset{\sim}{r}_f^{\pm} = \begin{Bmatrix} \rho\alpha_f \\ \pm\alpha_f c_f \\ \mp\alpha_s c_s \beta_y \,\mathrm{sgn}(B_x) \\ \mp\alpha_s c_s \beta_z \,\mathrm{sgn}(B_x) \\ 0 \\ \alpha_s\sqrt{\rho}c\beta_y \\ \alpha_s\sqrt{\rho}c\beta_z \\ \alpha_f \gamma p \end{Bmatrix} \qquad \underset{\sim}{l}_f^{\pm} = \begin{Bmatrix} 0 \\ \pm\dfrac{\alpha_f c_f}{2c^2} \\ \mp\dfrac{\alpha_s}{2c^2} c_s \beta_y \,\mathrm{sgn}(B_x) \\ \mp\dfrac{\alpha_s}{2c^2} c_s \beta_z \,\mathrm{sgn}(B_x) \\ 0 \\ \dfrac{\alpha_s}{2\sqrt{\rho}c}\beta_y \\ \mp\dfrac{\alpha_s}{2\sqrt{\rho}c}\beta_z \\ \dfrac{\alpha_f}{2\rho c^2} \end{Bmatrix} \tag{10}$$

-Slow magneto-acoustic waves: $\lambda_s = u_x \pm c_s$

Copyright © 2010 Asociación Argentina de Mecánica Computacional http://www.amcaonline.org.ar

$$\underset{\sim}{r}_s^{\pm} = \begin{Bmatrix} \rho\alpha_s \\ \pm\alpha_s c_s \\ \pm\alpha_f c_f \beta_y \operatorname{sgn}(B_x) \\ \pm\alpha_f c_f \beta_z \operatorname{sgn}(B_x) \\ 0 \\ -\alpha_f \sqrt{\rho} c \beta_y \\ -\alpha_f \sqrt{\rho} c \beta_z \\ \alpha_s \gamma p \end{Bmatrix} \qquad \underset{\sim}{l}_s^{\pm} = \begin{Bmatrix} 0 \\ \pm\dfrac{\alpha_s c_s}{2c^2} \\ \pm\dfrac{\alpha_f}{2c^2} c_f \beta_y \operatorname{sgn}(B_x) \\ \pm\dfrac{\alpha_f}{2c^2} c_f \beta_z \operatorname{sgn}(B_x) \\ 0 \\ -\dfrac{\alpha_f}{2\sqrt{\rho}c} \beta_y \\ \dfrac{\alpha_f}{2\sqrt{\rho}c} \beta_z \\ \dfrac{\alpha_s}{2\rho c^2} \end{Bmatrix} \tag{11}$$

-Magnetic flux wave: $\lambda_d = u_x$

$$\underset{\sim}{r}_d = \begin{Bmatrix} 0 \\ 0 \\ 0 \\ 0 \\ 1 \\ 0 \\ 0 \\ 0 \end{Bmatrix} \qquad \underset{\sim}{l}_d = \begin{Bmatrix} 0 \\ 0 \\ 0 \\ 0 \\ 1 \\ 0 \\ 0 \\ 0 \end{Bmatrix} \tag{12}$$

Where: $c_{A,n} = \dfrac{|B_x|}{\sqrt{\rho}}$;

$$c_{f,s}^2 = \frac{1}{2}\left(\frac{\gamma p + B^2}{\rho} \pm \sqrt{\left(\frac{\gamma p + B^2}{\rho} \right)^2 - 4\frac{\gamma p B_x^2}{\rho^2}} \right)$$

$$\beta_y = \begin{cases} \dfrac{B_y}{B_\perp} & B_\perp \neq 0 \\ \dfrac{1}{\sqrt{2}} & B_\perp = 0 \end{cases}$$

Copyright © 2010 Asociación Argentina de Mecánica Computacional http://www.amcaonline.org.ar

$$\beta_z = \begin{cases} \dfrac{B_z}{B_\perp} & B_\perp \neq 0 \\ \dfrac{1}{\sqrt{2}} & B_\perp = 0 \end{cases}$$

$$\beta_\perp = \sqrt{B_y^2 + B_z^2}$$

The Alfvén, entropy wave and magnetic flux waves, are linearly degenerate; hence the flow velocity is constant throughout the movement. The magneto-acoustic waves are nonlinear and can be shock or rarefaction waves. However, under particular relations between the magnetic field and the sound velocity theses waves may be locally non-convex (Courant and Fridrich, 1999; Serna, 2009).

3 NUMERICAL FORMULATION

To obtain the numerical solution of the system described by Eq.(2), a finite volume scheme has been implemented using a structured mesh, together with an approximate Riemann solver to calculate the fluxes with an explicit finite-difference scheme for the evaluation of the time evolution.

The numerical flows are evaluated by means of the Harten-Yee TVD technique, which allows the capturing of discontinuities, simultaneously achieving a second order approach (Yee, 1989).

The explicit TVD-finite volume scheme can be expressed as:

$$\boldsymbol{U}_{ij}^{n+1} = \boldsymbol{U}_{ij}^{n} - \Delta t \left[\frac{\overline{\boldsymbol{F}}_{i+\frac{1}{2};j}^{n} - \overline{\boldsymbol{F}}_{i-\frac{1}{2};j}^{n}}{\Delta x} \right] \tag{13}$$

where the function that determines the second-order numerical flux is defined as

$$\overline{\boldsymbol{F}}_{i+\frac{1}{2};j}^{n} = \frac{1}{2}\left(\boldsymbol{F}_{i+1}^{n} + \boldsymbol{F}_{i}^{n} + \left(\sum_{m} \boldsymbol{R}_{i+\frac{1}{2}}^{m} \Phi_{i+\frac{1}{2}}^{m} \right)^{(n)} \right) \tag{14}$$

The limiter function used is one of minmod type,

$$\Phi_{i+\frac{1}{2}}^{m} = \left(g_{i+1}^{m} + g_{i}^{m} \right) - \psi\left(\lambda_{i+\frac{1}{2}}^{m} + \gamma_{i+\frac{1}{2}}^{m} \right) \alpha_{i+\frac{1}{2}}^{m} \tag{15}$$

Copyright © 2010 Asociación Argentina de Mecánica Computacional http://www.amcaonline.org.ar

$$g_i^m = \mathrm{sgn}\left(\lambda_{i+\frac{1}{2}}^m\right)\max\left\{0, \min\left[\sigma_{i+\frac{1}{2}}^m \left|\alpha_{i-\frac{1}{2}}^m\right|, \sigma_{i-\frac{1}{2}}^m \frac{\mathrm{sgn}\left(\lambda_{i+\frac{1}{2}}^m\right)}{2}\alpha_{i-\frac{1}{2}}^m\right]\right\}; \quad \sigma_{i+\frac{1}{2}}^m = \sigma\left(\lambda_{i+\frac{1}{2}}^m\right) \tag{16}$$

$$\gamma_{i+\frac{1}{2}}^m = \begin{cases} \dfrac{1}{\alpha_{i+\frac{1}{2}}^m}\left(g_{i+1}^m - g_i^m\right) & \alpha_{i+\frac{1}{2}}^m \neq 0 \\ 0 & \alpha_{i+\frac{1}{2}}^m = 0 \end{cases} \tag{17}$$

Approximate Roe-type Riemann solver produces only shock waves so a physically correct smooth rarefaction wave is replaced by a rarefaction shock wave that violates the entropy condition. An alternative to correct this non-physical solution is using a “sonic entropy fix” that smoothes out eigenvalues in the vicinity around zero. Harten (1982) suggested an entropy fix for Roe’s method, which has been widespread used:

$$\psi(z) = \begin{cases} |z| & |z| \geq \delta \\ \dfrac{1}{2\delta}\left(z^2 + \delta^2\right) & |z| < \delta \end{cases} \tag{18}$$

The function ψ in Eq.(15) is an entropy correction to z, whereas δ is generally a small and constant value that needs to be calibrated for each problem. A proper choice of the entropy parameter δ for higher Mach number flows helps in preventing nonphysical solutions and can act, in some sense, as a control of the convergence rate and the sharpness of shocks (Yee, 1989).

For time-accurate calculations in explicit numerical algorithms

$$\sigma(z) = \frac{1}{2}\left[\psi(z) - \frac{\Delta t}{\Delta x} z^2\right] \tag{19}$$

and the wave strength of the m-th wave is

$$\alpha^m = \boldsymbol{L}^m \cdot \left(\boldsymbol{W}_{i+1} - \boldsymbol{W}_i\right) \tag{20}$$

where $\boldsymbol{L}^m$ is the left eigenvector for the m-th wave and $\boldsymbol{W}$ represents the primitive variable vector.

4 MODEL

We perform two set of partially independent simulations. One of them in the sunwards direction, and the other directed transversally to them. The coordinate *x* represents the sunward direction and the *y* coordinate is transverse to the magnetic field one. We chose as test case the edge C observational parameters taken from Verwichte *et al.* (2005), shown in

Copyright © 2010 Asociación Argentina de Mecánica Computacional http://www.amcaonline.org.ar

Table 1. The non–dimensional quantities used for the numerical simulations are the ratios of a dimensional quantity and a reference one. We assume an initial ratio of pressure values and a characteristic background density, the reference value $\rho_{ref.}$ Figure 1 exhibits the geometrical used model for both set of numerical simulations.

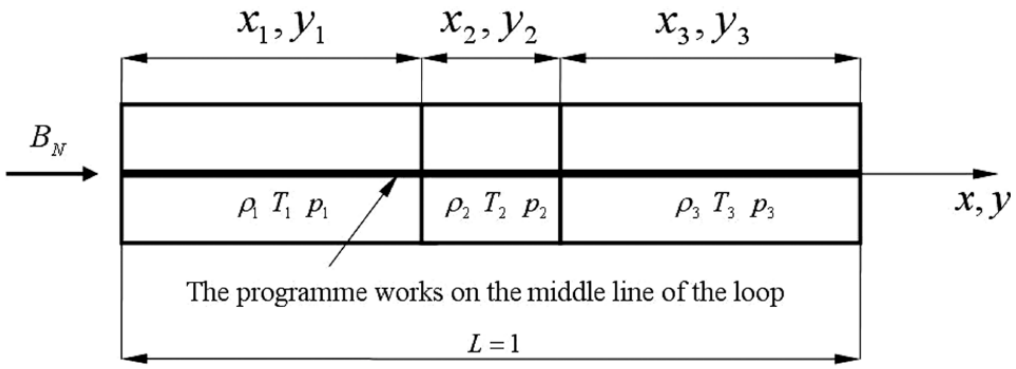

Figure 1. Geometry of the model. The same geometry is implemented for the *x* and *y* coordinates

N^o	1	2 (test)	3	4	5	6
τ (s)	91	134	182	182	175	217
A (km)	328	906	811	594	246	375
$V_{\rm ph}$(km s^{-1})	220	202	171	218	176	110

Table 1. Observational parameters for Verwichte *et al.* (2005). τ is the period, V_{ph} is the sunward observational phase speed and *A* is the amplitude.

Edge	y_1, y_2, y_3	$P_2/P_{1,3}$	x_1, x_2, x_3
C(transverse)	0.7, 0.04, 0.26	20	–
C(radial)	–	20	0.7, 0.25, 0.05

Table 2. Initial condition values for the transverse pattern simulation shown in Figs. 2 and for the sunward pattern simulation shown in Fig. 3c. The initial non-dimensional conditions are $p_1 = p_3$, $\rho_1 = \rho_2 = \rho_3 = 1$.

The other reference values are derived from the following calibration procedure. For the transverse shock we perform the iteration:

(i) We chose B_{ref} as the background magnetic field value of the test case, thus B_{ref} must satisfy the condition $\beta < 1$ (in our tests $\beta = 0.1$). The reference value of the magnetic pressure is $p_{ref} = B^2_{ref}/2\mu_o$.

(ii) From the numerical transverse simulation (*e.g.*, Fig. 2a) we obtain the reference

Copyright © 2010 Asociación Argentina de Mecánica Computacional http://www.amcaonline.org.ar

amplitude A_{ref} and the reference period τ_{ref} ; $\tau_{ref} = \tau/\tau_n$ and $A_{ref} = A/A_n$; being τ and A the observational values for the amplitude and period of the test case in Table 1. τ_n and A_n are the non–dimensional amplitude and period taken from the simulation. Figure 2a corresponds to the last step of the iteration and gives the numerical density of the resulting transverse perpendicular magnetic shock pattern, using the initial conditions given in Table 2 (first line).

(iii) The non–dimensional velocity, amplitude and period are related by the expression, $V_n = 2A_n/\tau_n$. The reference velocity is determined from the correspondent dimensional speed $V = V_n\, V_{ref} = 2A/\tau$ as $V_{ref} = 2A/(\tau\, V_n)$

(iv) If the reference magnetic field satisfies $V_{ref} = B_{ref} / \sqrt{\mu_o \rho_{ref}}$; the iteration finishes. If not, new elections of B_{ref} are accomplished, giving new numerical determinations of A_n/τ_n and V_n, until the relation holds.

(v) Then, the reference temperature value is obtained using the state equation for atomic hydrogen: $p_{ref} = R\, \rho_{ref}\, T_{ref}$.

Using this procedure we obtain the reference values of the transverse simulations for the test case. For $\rho_{ref} = 2\text{x}10^{-11}\text{kg/m}^3$; the resulting reference values are $B_{ref} = 20\text{G}$, $p_{ref} = 1.6\text{Pa}$, $T_{ref} = 9\text{x}10^6\text{K}$ and $V_{ref} = 188\text{km/s}$; $A_{ref} = 12943\text{km}$ and $\tau_{ref} = t_{ref} = 69\text{s}$ correspond to the non–dimensional values $A_n = 0{:}07$ and $\tau_{ref} = t_n = 1.95$ obtained from Fig. 2a. These values are also used for the sunward simulation modeled as a pressure perturbation is localized at the partition y_2 (corresponding to $L_v = 50\text{Mm}$) of the whole interval $y = (y_1; y_2; y_3)$ (see Table 2). The background gas pressure of the corona is $p_1 = p_3$.

5 RESULTS

We carried out two different group of simulation, one for sunward direction, and other for transverse direction.

5.1 Transverse perpendicular magnetic shocks

Figures 2a-d show, respectively, the numerical results of the density, temperature, magnetic pressure and gas pressure patterns of the test case as a function of time. The void, that satisfies the edge C description in Verwichte *et al*. (2005), is the result of a nonlinear evolution of waves triggered by the instantaneous initial pressure pulse that excites the whole pattern. We note that the perturbation, seen as a transverse to the field line phenomenon, produces opposite magnetic shock waves that bounce in the lateral and denser boundary medium. The resulting oscillatory pattern of interacting nonlinear waves composes a void cavity which is sustained for a time interval adjusting the observations. In accordance with McKenzie (2000), Figs. 2a-b show that the moving voids consist of a low–density and high–temperature plasma with respect to the surrounding medium.

Copyright © 2010 Asociación Argentina de Mecánica Computacional http://www.amcaonline.org.ar

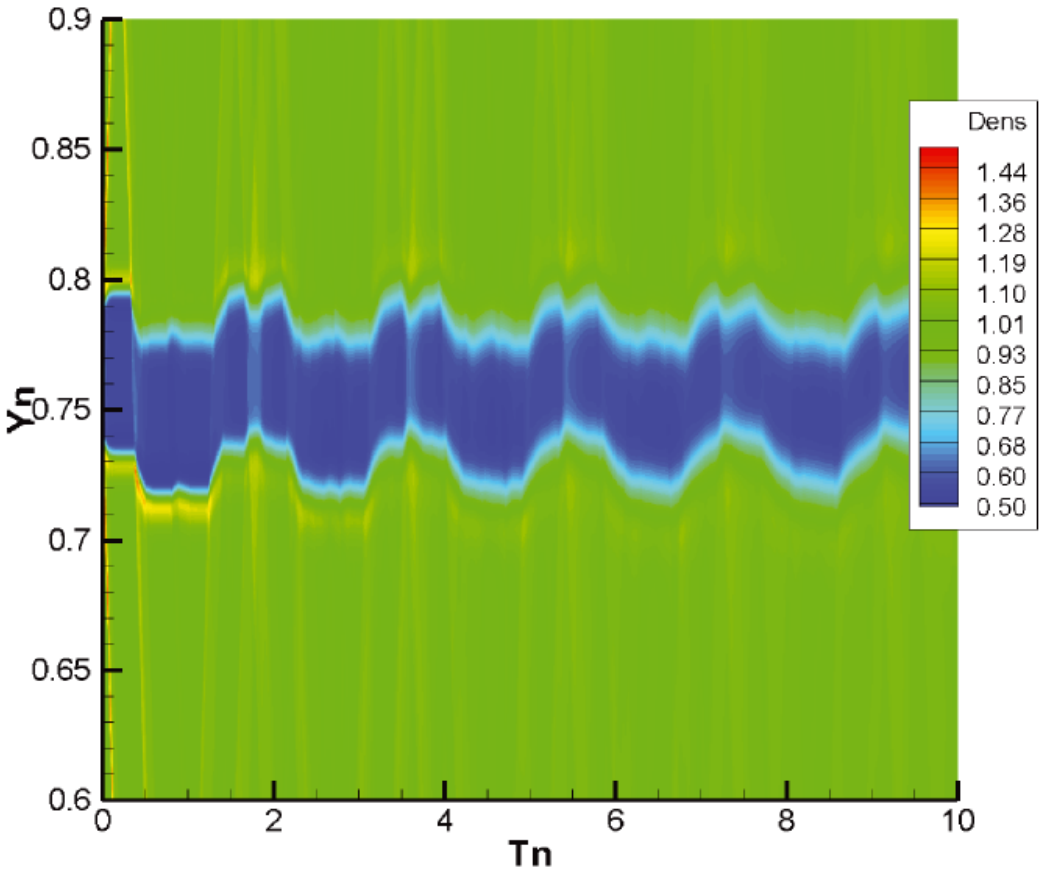

Figure 2a. Evolution of the non-dimensional density. Dimensional values can be obtained multiplying by A_{ref} = 33556km, t_{ref} = 67s and $\rho_{ref} = 10^{-12}$ kg/m^3.

Figure 2c exhibits that the magnetic pressure is lower inside the void than in the external medium. However, due to the larger temperature values inside the void, it results that the inner gas pressure (see Fig. 1d) compensates the lower magnetic pressure, both of which equilibrate the lower gas pressure plus the larger magnetic pressure of the outside media, the total inside pressure ($P_g + P_{mag}$), which equals the total outside pressure, $(P_g + P_{mag})_{out}$'. Thus, our simulations allow a description of the phenomenon where the void cavity is a $\beta > 1$ perturbed region generated by the non–linear interaction of transverse waves. In this sense the void can be thought of as an emergent property of the collective and non–linear plasma interactions.

5.2 Radial hydrodynamic shocks

In the radial direction the pressure pulse is supposed to be associated with an upward reconnection event, from where field lines slowly retract away under the force of magnetic tension (McKenzie 2000). The pulse generates shocks traveling sunwards and outwards, along the magnetic field lines. The nonlinear interaction of outward rebound waves, near the reconnection site, and sunward absorbed ones compose an overall descending void structure.

Copyright © 2010 Asociación Argentina de Mecánica Computacional http://www.amcaonline.org.ar

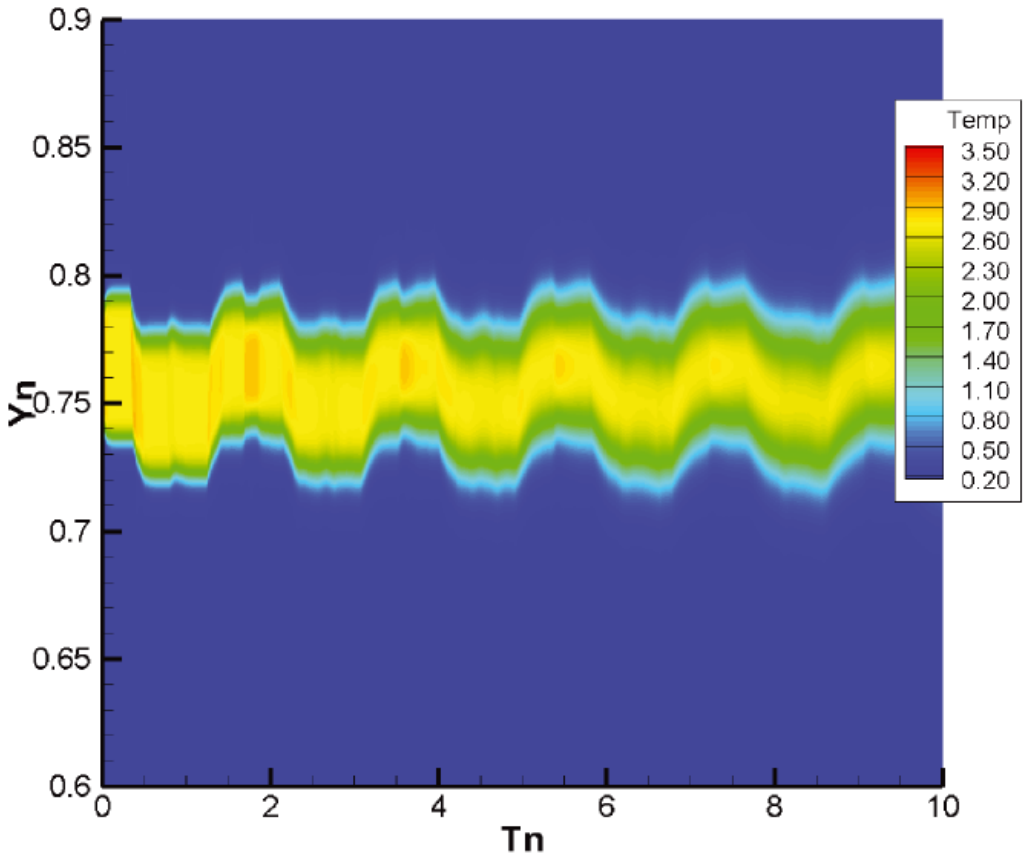

Figure 2b Evolution of the non-dimensional temperature. Dimensional values can be obtained multiplying by A_{ref} = 33556km, t_{ref} = 67s and $T_{ref} = 3.10^6$ K.

Figure 3a-c gives numerical results obtained varying the pressure pulse: p_2/p_1 = 2; 5 and 20; respectively. In accordance with the assumption that in the radial direction the role of the magnetic field is to guide the interacting hydrodynamic waves the figures are not modified when the magnetic field intensity is varied. Figure 3c, equivalent to Figure (2C) in Verwichte *et al.* (2005), corresponds to the test case. The sunward perturbation is absorbed by the denser media nearer to the sun surface. The upward moving shock is forced to rebound at x_n = 1: The interaction of the subsequent waves composes a downward moving void as it is indicated in the figures by the color contrast, i.e. darker features correspond to lower values of the density.

Non-linear wave interactions generate a region of low density that is separated from a vacuum upper zone, also formed by the interaction of nonlinear upward and downward moving perturbations. This intermediate vacuum zone can be clearly appreciated in Figs. 3a-b. For these cases the jump in the density discontinuity is less pronounced. It is interesting to note the similarity between the numerical results and Figs. 2c-d in Verwichte *et al.* (2005).

To compare our sunward speed values with those in Verwichte *et al.* (2005) we calculated the velocity of the curve limiting the vacuum zone. Figure 4 shows the good accordance between the test numerical case for p_2/p_1 = 20 and the correspondent observational curve.

Copyright © 2010 Asociación Argentina de Mecánica Computacional http://www.amcaonline.org.ar

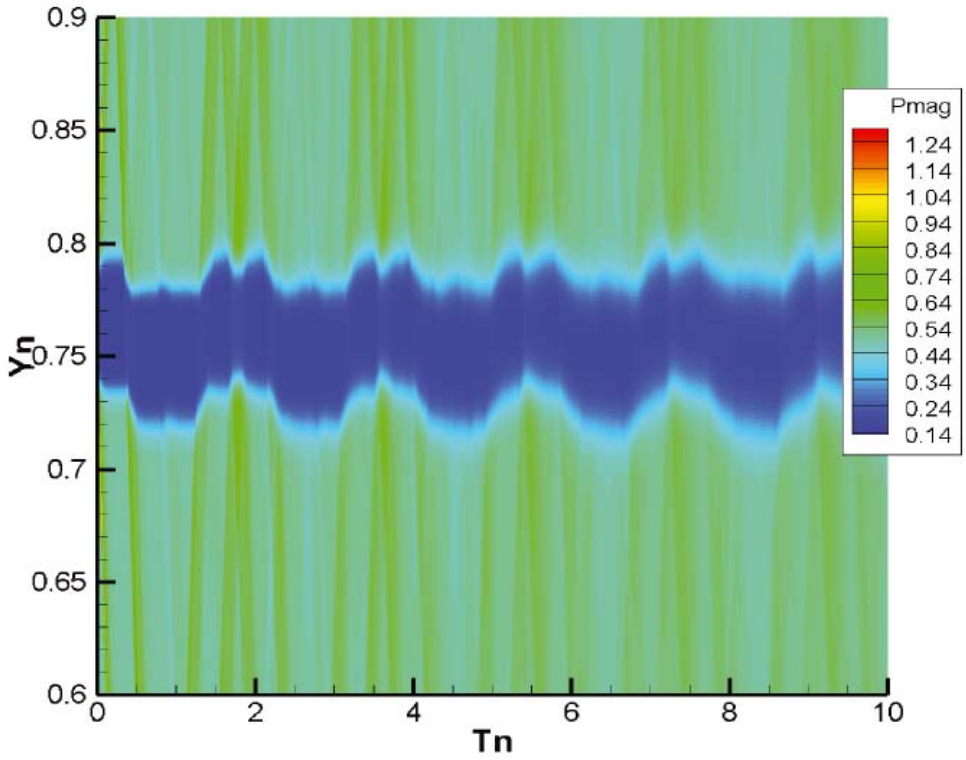

Figure 2c Evolution of the non-dimensional magnetic pressure. Dimensional values can be obtained multiplying by A_{ref} = 33556km, t_{ref} = 67s and p_{ref} = 0.25Pa.

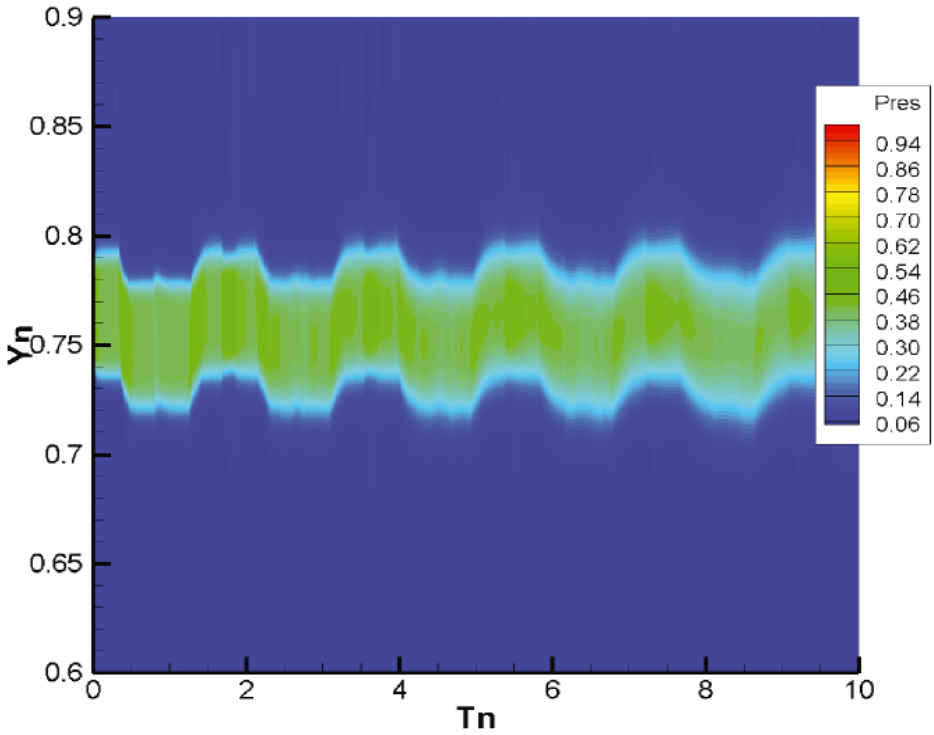

Figure 2d. Evolution of the non-dimensional mechanic pressure. Dimensional values can be obtained multiplying byA_{ref} = 33556km, t_{ref} = 67s and p_{ref} = 0.25Pa.

Copyright © 2010 Asociación Argentina de Mecánica Computacional http://www.amcaonline.org.ar

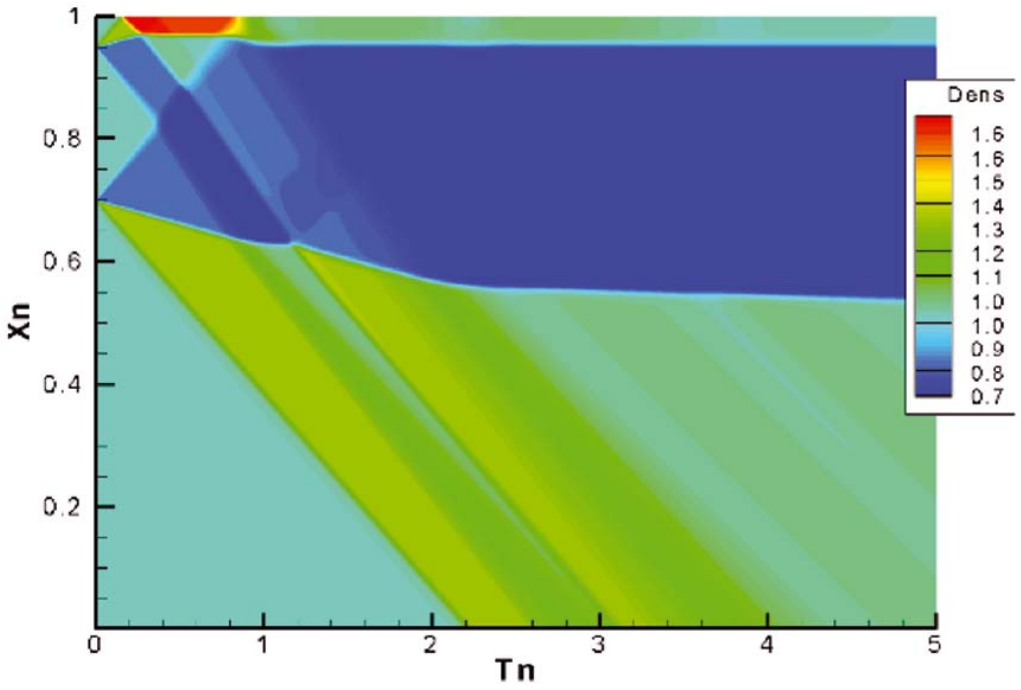

Figure 3a. Radial simulation for $p_2/p_1 = 2$. $x_n = 0.7$ corresponds to $L_v = 50$ Mm and $t_{ref} = 67$s

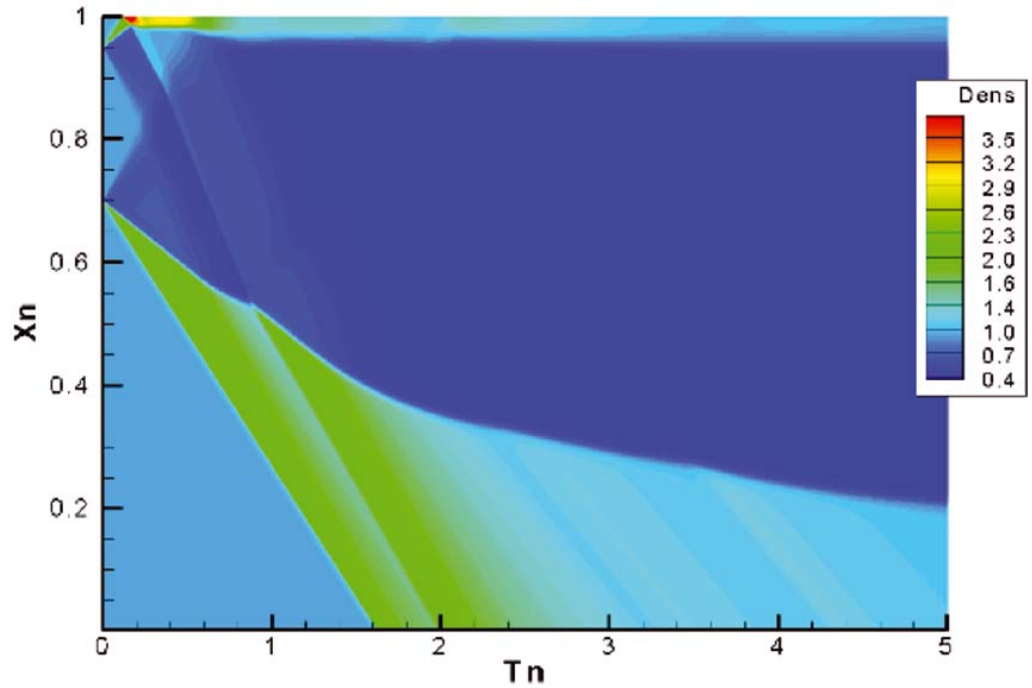

Figure 3b. Radial simulation for $p_2/p_1 = 5$. $x_n = 0.7$ corresponds to $L_v = 50$ Mm and $t_{ref} = 67$s

Copyright © 2010 Asociación Argentina de Mecánica Computacional http://www.amcaonline.org.ar

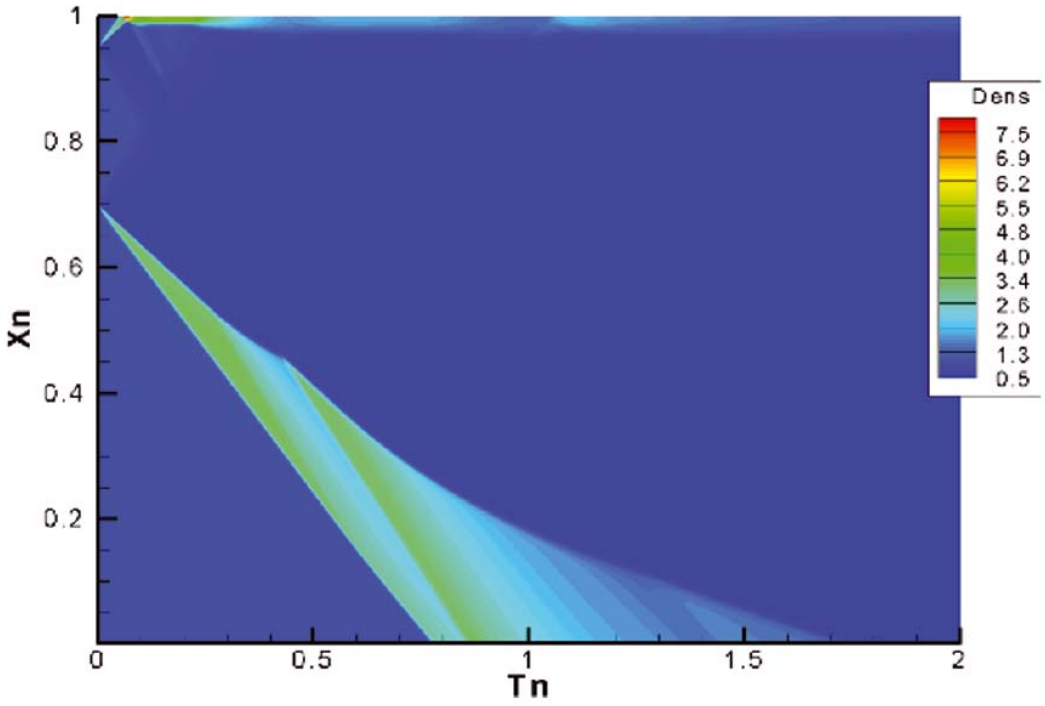

Figure 3c. Radial simulation for $p_2/p_1 = 20$. $x_n = 0.7$ corresponds to $L_v = 50$ Mm and $t_{ref} = 67$s

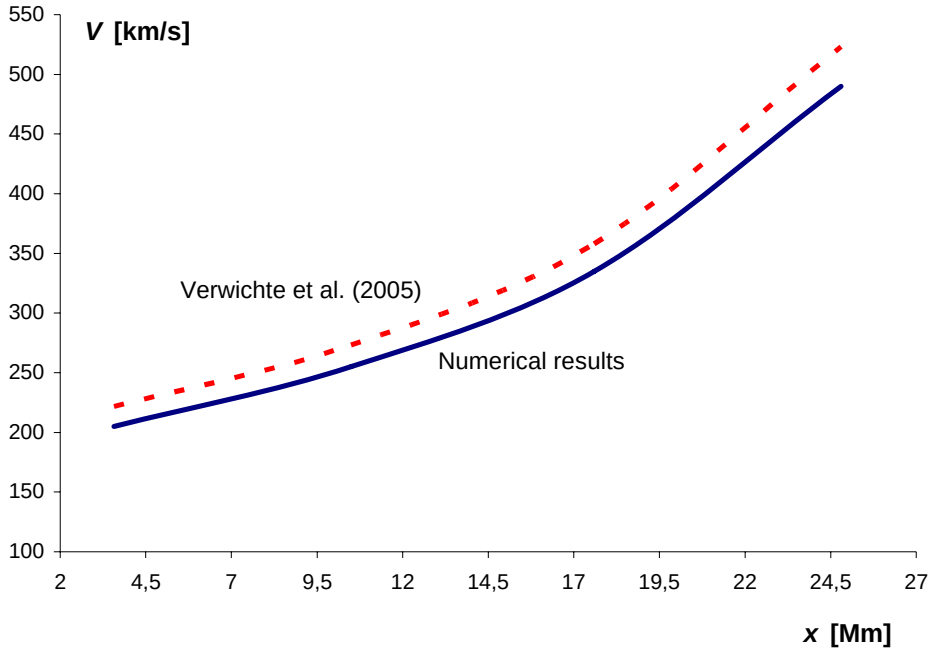

Figure 4. Comparison between the radial velocity obtained by numerical simulation and experimental measurements as function of the sunward distance for $p_1/p_2 = 20$.

Copyright © 2010 Asociación Argentina de Mecánica Computacional http://www.amcaonline.org.ar

6 CONCLUSIONS

We have integrated the ideal magnetogasdynamics equations to simulate observational solar dark lane data. We simulated the effects of an initial impulsive and localized deposition of energy – supposed to be associated with above reconnection processes – in a structured plasma by sunward magnetic field lines. The impulsive phase is modelled by a pressure perturbation that initiates two main different types of processes, a fundamentally hydrodynamic shock pattern directed sunwards and a perpendicular magnetic shock one, i.e. transversal to the magnetic field. The two patterns are supposed to be semi-independent processes.

To solve the magnetogasdynamics equations we have implemented a finite volume method together the Harten-Yee TVD scheme to calculate the numerical flux. The eight-wave technique introduced by Powell (1995) was used and the eigenvectors are normalized according to Zarachay, *et al.* (1994) and Roe (1996).

We were able to calibrate the oscillatory behavior in the transverse direction and reproduce observational measurements. The void structures are produced by the rebounds of the magnetic transverse shocks in the denser external medium. The resulting interactions of bounced non-linear shocks compose and sustain, in accordance with observational characteristic times of the phenomenon, a density structure with a central void.

The same reference values were used as initial condition to simulate the sunward evolution. We could qualitatively reproduce the observational data showing that initially two opposite shock evolving fronts are produced. One evolves towards the Sun surface until is absorbed, and the other is forced to rebound upwardly resembling the action of a reconnection site. Afterwards, the interaction of upwardly and downwardly moving perturbations forms an expansion wave region that lowers the density of the medium. Furthermore, a voided zone is formed and sustained due to the continued interfering of nonlinear waves.

Acknowledgments.
This work was supported by the SECyT of the National University of Córdoba, CONICET and MCyT Córdoba.

REFERENCES

Asai A., Yokoyama T., Shimojo M., MHD Simulations of a Moving Subclump with Heat Conduction, *Journal of The Korean Astronomical Society*, 37: 575–578, 2004

Costa, A.; Elaskar, S.; Fernández, C. y Martínez, G., Numerical simulation of dark inflow in post-flare-supra-arcade. *Monty Notice Royal Astronomy Society* 400: L85–L89, 2009.

Courant, R. and Friedrich, K., *Supersonic Flow and Shock Waves*, Springer, New York, 1999.

Elaskar, S. and Brito, H., Numerical solution of the magnetogasdynamics equations as a tool for the design of pulsed plasma thruster. *Proceedings International Electric Propulsion Conference 2001*, IEPC-01-141, Passadena. USA, 2001.

Fernández C., Costa A., Elaskar S., Schulz W., Numerical simulation of the internal plasma dynamics of post-flare loops. *Monty Notice Royal Astronomy Society*, 400: 1821–1828, 2009.

Goldston, R. and Rutherford, P., *Introduction to Plasma Physics*, Institute of Physics

Copyright © 2010 Asociación Argentina de Mecánica Computacional http://www.amcaonline.org.ar

Publishing, London, 2003.

Harten, A., High resolution schemes for hyperbolic conservation laws, Courant Mathematics and Computing Laboratory, *U.S. Department of Energy, DOE/ER/03077-175*, 1982.

Innes D. E., McKenzie D., Wang T., Observations of 1000 km s^{-1} Doppler shifts in 10^7 K solar flare supra-arcade, *Solar Physics*, 217, 267-279, 2003a

Innes D. E., McKenzie D., Wang T., SUMER spectral observations of post-flare supra-arcade inflows, *Solar Physics*, 217: 247–265, 2003b.

Kirk J., Melrose D. and Priest E., *Plasma Astrophysics*, Springer-Verlag, Berlin, 1994.

Maglione L. ; Elaskar, S.; Brito, H.; Dean, R. and Lifschitz, L., A software engineering for numerical simulation of 2D non-stationary real MGD flows, *Proceeding of Applied Mathematics and Mechanics Journal*, ISSN 1617-7061, 7 (1): 2010027-2010028, 2007.

McKenzie D., Velocity Fields and Structure above LDE arcades: Possible Observational Signatures of Reconnection, *Solar Physics*, 195: 381-385, 2000

McKenzie D., Savage S., Quantitative Examination of Supra-arcade Downflows in Eruptive Solar Flares, *The Astrophysical Journal*, 697: 1569-1577, 2009

Powell, K., An approximate Riemann solver for magnetohydrodynamics (that works in more than one dimension), *NASA Contract No NAS1-19480*, 1995.

Roe, P., and Balsara, D., Notes on the eigensystem of magnetohydrodynamics, *SIAM Journal of Applied Mathematics*, 56: 57-67, 1996.

Schulz, W., Costa, A., Elaskar, S. and Cid, G. Simulation of dark lanes in post–flare supra–arcades, II. A contribution to the remote sensing of the coronal magnetic field, *Monty Notice Royal Astronomy Society*, 407: L89-L94, 2010**.**

Serna, S. A characteristic-based nonconvex entropy-fix upwind scheme for the ideal magnetohydrodynamic equations, *Journal Computational Physics*, 228 (11): 4232-4247, 2009.

Verwichte E., Nakariakov V., Cooper F., Transverse waves in a post-flare supra-arcade, *Astronomy and Astrophysics*, 430: L65-L69, 2005

Yee, H., A Class of High-Resolution Explicit and Implicit Shock-Capturing Methods. *NASA Technical Memorandum 101008*, Ames Research Center, California, 1989.

Zarachay, A., Malagoli, A., and Collela, P., A higher order Godunov method for multidimensional ideal magnetohydrodynamics, *SIAM Journal of Scientific Computation*, 15: 263-284, 1994.

Copyright © 2010 Asociación Argentina de Mecánica Computacional http://www.amcaonline.org.ar